Turbulence Structure and Large-Scale Unsteadiness in Shock-Wave / Boundary Layer Interaction

Kevin M. Porter* and Jonathan Poggie†
Purdue University, West Lafayette, IN 47906

The effects of unsteady separation on the structure of a turbulent boundary layer were explored using wall-resolved, implicit large eddy simulation. The configuration used for this computation was a compression ramp of 24 degrees in a Mach 2.25 flow. This configuration was chosen because it has been shown to undergo shock-induced separation in previous work. A turbulent boundary layer was generated by imposing an artificial body force trip on a laminar boundary layer, and allowing it to develop into a fully turbulent flow. The resulting static pressure profile, skin friction coefficient, and boundary layer profile showed good agreement with other computations run at the same conditions. Data were recorded before and after the shock-wave / separation system to observe the changes in turbulence statistics. The effects on the Reynolds stresses were of particular interest for application in turbulence modeling. Large-scale, low-frequency pressure fluctuations caused by unsteadiness of the initial shock were also evaluated.

Nomenclature

x	Streamwise direction
y	Wall normal direction
z	Spanwise direction
u,v,w	Velocities in the x, y, and z directions
C_f	Skin friction coefficient
Re	$U_\infty \ell / \nu_\infty$, Reynolds number
p	Non-dimensional static pressure
M	Mach number
δ	Boundary layer height corresponding to $0.99\,U_\infty$
T	Non-dimensional static temperature
ρ	Non-dimensional density
N	Number of points
$\langle\rangle$	Mean values
θ	Boundary layer momentum thickness
St	$f\ell/U_\infty$, Strouhal number
u_τ	$\sqrt{\tau_w/\rho_w}$, wall friction velocity
Superscript	
$+$	Normalized using inner units
$\prime$	Fluctuating components
Subscripts	
w	Wall value
∞	Freestream values
o	Initial Values

I. Introduction

Supersonic compression ramps and the associated shock-wave / boundary-layer interactions (SBLI) have been a topic of study for many decades. Shock-wave / boundary-layer interactions are a critical area of study because of their prevalence in real-world, high-speed flight vehicles. These interactions occur anywhere a shock wave intersects the surface of the vehicle, and if the shock wave is strong enough, can give rise to an area of separation. It has been observed that the shock-wave / separation system can oscillate at a low frequency, and with a large length scale, compared to the boundary layer. This oscillation frequency is often close to the resonant frequencies of the structure of the flight vehicle and can be a concern to designers. The interaction also gives rise to increased turbulent motion in the boundary layer. Experiments studying some of the canonical cases of this interaction have been carried out since the 1950's.[1,2] Computations of these flows have become routine in more recent years, as computational resources and methods have advanced to the point where it is viable to perform LES or DNS on these cases.[3,4]

This paper is an exploration of wall-resolved, implicit large eddy simulation (effective DNS) of a compression corner case at Mach 2.25. The first section of the paper gives a brief background of experimental and computational

*Graduate Research Assistant, School of Aeronautics and Astronautics, Student Member AIAA.
†Associate Professor, School of Aeronautics and Astronautics, Associate Fellow AIAA.

work done on SBLI on compression corners. The second section describes the computational setup of the calculations done for this paper. The flow solver and grid details are summarized in this section as well as the boundary and initial conditions. The third section gives the results of the simulation. The basic characteristics of the turbulent boundary layer are reported in order to establish good agreement with previous work and establish a well-developed boundary layer as the inflow boundary condition. The spanwise profiles of important variables are reported as well as some general images of the flow structure. Fourth, a more in-depth survey of the turbulent structures and low frequency oscillations is included in the paper. Finally, conclusions are made about this computational study and possible future work explored.

This simulation sets the stage for future investigations in controlling the scale and frequency of the oscillations. One method of control could consist of using plasma actuators to introduce momentum into the boundary layer to delay separation.[5] The goal of any method of control is not necessarily to entirely eliminate the region of separation, but rather to move the frequency of the oscillation away from critical structural frequencies by manipulating the separated region.

I.A. Background

There is a rich experimental and computational history in shock-wave / boundary layer interactions. This topic has been the focus of extensive wind tunnel experiments since the 1950's.[2] Significant progress has been made since then in observing and cataloging SBLI and its effects. Settles et al.[6] investigated the effect of the compression ramp angle on the size of the separated region. The work Smits and Muck[1] focused on the implications of the interaction on the amplification of Reynolds stresses. Unsteadiness has also been observed and studied experimentally.[7] This observed unsteadiness has been the focus of recent work as it has real world impacts on flight vehicle design. Recently, work has been focused on controlling the interaction with a variety of techniques. Methods such as air-jets, vortex generators, and plasma actuators are being experimentally investigated as ways to reduce the unsteadiness associated with SBLI.[8–10] Each of these methods of control has advantages and disadvantages, and can be difficult to test in the wind tunnel given the nature of the flowfield.

As computational power and numerical techniques have improved, high resolution computations have become possible for the separated compression corner. The first of these studies was performed by Adams[4] in 2000 on a $18\,\mathrm{deg}$ compression ramp. Since this first foray into computational investigations of SBLI, there have been many additional studies on this problem. Attempts have been made to combine LES and RANS in order to make analysis less costly.[11] Most of the early computational work on this subject has been at a low Reynolds number due to the computational expense of higher Reynolds number flow calculations.

Turbulence amplification caused by shock boundary layer interaction has been observed in both experiments and simulations.[1,3] The amplification of turbulence is of engineering interest as it can affect heat transfer and skin friction. In their paper, Wu and Martin[3] showed an increase of about three times in the $\langle u\prime u\prime \rangle$ component of Reynolds stress, and a factor of 20 in the other components.

Large-scale, low-frequency unsteadiness has also been a focus of shock-wave/boundary layer research in both experiments and computations. A comprehensive review of the experimental work done on this unsteadiness can be found in a paper by Dolling.[12] It has been observed that the frequency of the oscillation tends to be about $fL_{sep}/U_\infty = 0.01$ to 0.03, where L_{sep} is the size of the separated region.[5]

II. Model

II.A. Grid and Code

The code used to perform the computations was the Higher Order Plasma Solver, or HOPS. HOPS is a structured-grid solver for the Navier-Stokes equations. More information about the HOPS code can be found in Ref. 13, where its performance is compared to that of the codes FDL3DI and US3D for a flat plate turbulent boundary layer. The time integration scheme used here was a second-order implicit method with quasi-Newton subiterations. For the spacial discretization scheme, a sixth-order compact difference method was used. A shock detection routine was used, and an upwind scheme was used for cells in the vicinity of a shock.

The calculations were conducted on a three-dimensional, structured grid as shown in Figure 1, the dimensions of which are shown in Table 1. Care was taken to ensure that the grid was orthogonal to the wall near the boundary and parallel to the flow, but the corner in the configuration required that some boundary cells were non-orthogonal to avoid intersecting lines or highly skewed cells. The top of the grid was created at a steeper angle than the compression

corner in order to properly align the grid in the domain with the shock-wave. There was a buffer layer in both the x- and y-directions where the grid was stretched in order to minimize reflections back into the domain.

Parameter	Value
δ_0	6.096×10^{-4} m
$L_x \times L_y \times L_z$	$140\delta_0 \times 30\delta_0 \times 10\delta_0$
$N_x \times N_y \times N_z$	$6451 \times 1021 \times 453$
N(Total)	2.9×10^9
$\Delta y^+_{BL_{edge}}$	2.27
Δy^+_w	.515
Δx^+	5.15
Δz^+	5.15

Table 1: Grid Parameters. Values in wall units ($+$) calculated at $80\delta_0$, just before the initial shock.

The grid had constant spacing in the x and z direction but coarsened away from the wall in the y direction. The grid was periodic in the z direction with a domain size of $10\delta_0$, which has been shown to be large enough to decorrelate the center of the domain with the edge for a flat plate turbulent boundary layer under similar flow conditions.[14] The adequacy of the domain width for separated flow is being investigated in the current work. The grid fell well within the range accepted as wall-resolved, implicit large-eddy simulation: the Δx^+ and Δz^+ spacing were both less than ten, and the Δy^+ at the wall was less than one.[15]

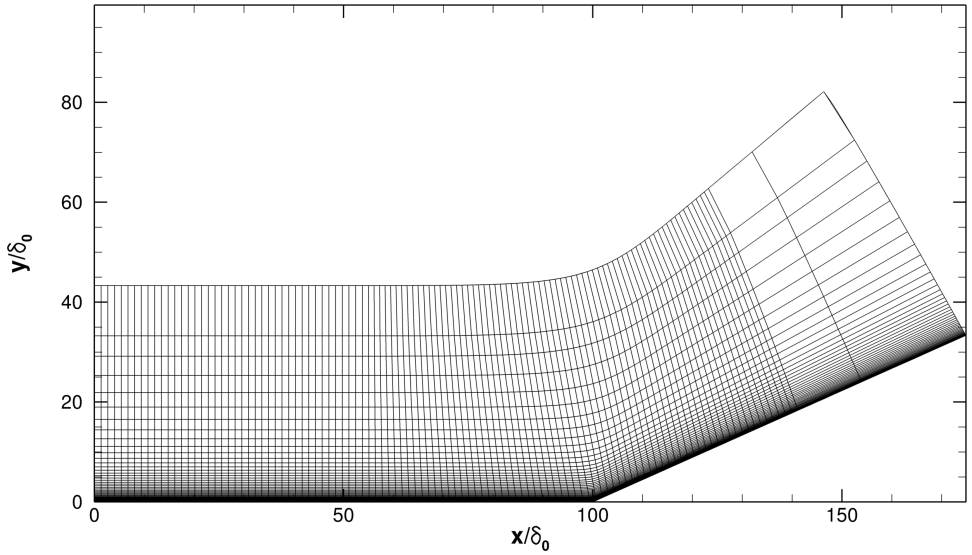

Figure 1: Grid on which computations were done. Some points were removed for clarity.

II.B. Flow Characteristics

Table 2 presents the conditions at which the simulations were run. These conditions mirror those in the paper by Bisek et al.[5] Matching the conditions of this previous work allowed for comparison of the computational results. That simulation showed significant shock induced separation, a desired trait for this study. These conditions have also been used in other studies of shock-wave/boundary layer interaction.[16,17]

The inlet boundary condition for the computation was a laminar boundary layer profile, and the flow was transitioned to turbulence by way of an artificial body force trip applied near the inlet. Details of the body force trip method can be found in the paper by Mullenix et al.[18] A non-slip, isothermal wall boundary condition was used for the surface of the ramp. Outflow boundaries were used for the top and outlet of the domain. The z-direction of the domain is periodic.

Parameter	Value
U_∞	588 m/s
M	2.25
T_∞	170 K
T_w	323 K
p_∞	2.383×10^4 Pa
Re_θ	3100
δ_0	6.096×10^{-4} m

Table 2: Flow conditions for $24\,\mathrm{deg}$ compression ramp.

The initial condition for this case was a uniform flow in the domain. The time step used in the calculation was $\Delta t U_\infty/\delta_0 = 0.01$ which was equivalent to a $\Delta t^+ = 0.11$. Investigations of the effect of time step on turbulent boundary layers showed little of effect of changes in Δt^+ in this range.[19] The calculations were run for an extended period of time, about 4.5 domain flow-through times, before any data was collected in order to allow the flow to evolve past the initial transients.

III. Results

III.A. Turbulent Inflow

Before investigating the effects of the shock-wave/boundary layer interaction and the large scale unsteadiness, it was important to establish that a well developed turbulent boundary layer had been achieved. As mentioned in the previous section, a laminar profile was imposed on the inlet condition, and transition was promoted by a body force trip. The turbulent boundary layer was allowed to develop over approximately 80 initial boundary layer thicknesses downstream.

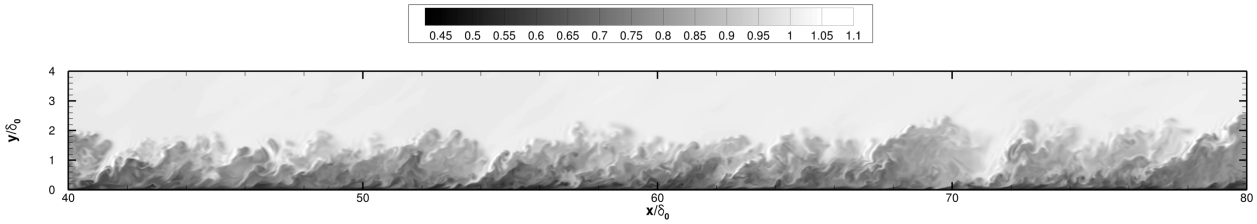

Figure 2: Normalized density contour plot of turbulent boundary layer upstream of interaction region.

Figure 2 shows the density field in the $z/\delta_0 = 5$ plane for the fully developed turbulent boundary layer upstream of the separated region. It was about two initial boundary layer heights tall, with the ejections reaching around three times the initial boundary layer height. The location shown in Figure 2 at $80\delta_0$ was the where the pre-SBLI data of the boundary layer were recorded. To verify that the boundary layer had fully developed to turbulence, the current simulation was compared to other LES work and to experiments and theory. In particular, the results obtained in the present study were compared to data from Ref. 19, which reported a computation with FDL3DI for the same flow parameters as the current case.

The Van Driest transform of the incoming boundary layer profile taken at $x = 80\delta_0$ showed good agreement with the theoretical predictions for turbulent boundary layers. It also compared well with previous computations of this flow as well as experimental data. There was a slight under prediction of the u^+ value at the outer edge of the boundary layer, but the shape of the profile matched well with both the experiments and computations.

The Reynolds stress amplification was a parameter of interest for this study, so it was important to verify that the incoming boundary layer had correct Reynolds stress profiles. The current simulation was compared to the turbulent boundary layer simulation of Poggie[19] and the experiments of Éléna and Lacharme.[20]

The current study agreed well with both the previous LES simulations and the experimental data. The magnitude of the maximum $\rho\langle v'^2\rangle$ values differed somewhat with the Elena experiment but overall, the trend was the same.

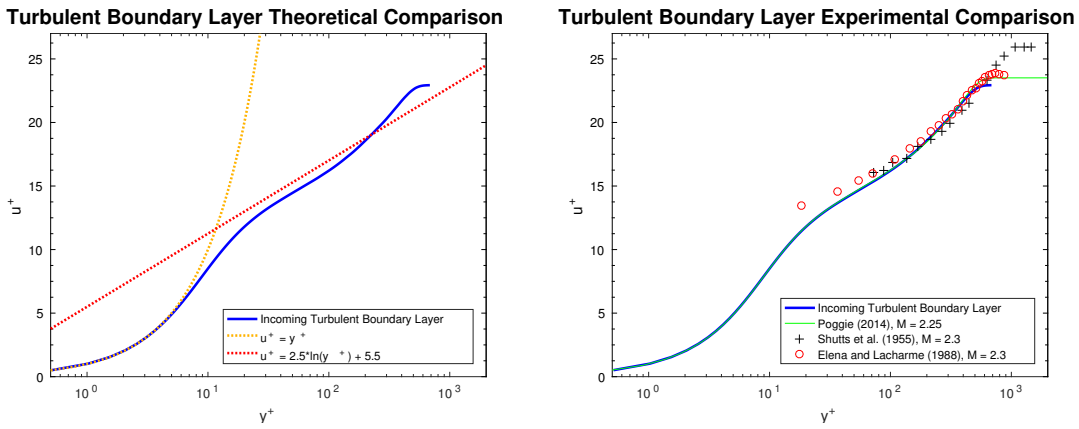

(a) Comparison to theory.

(b) Comparison to experiments.

Figure 3: Van-Driest transformation of incoming boundary layer mean velocity profile.

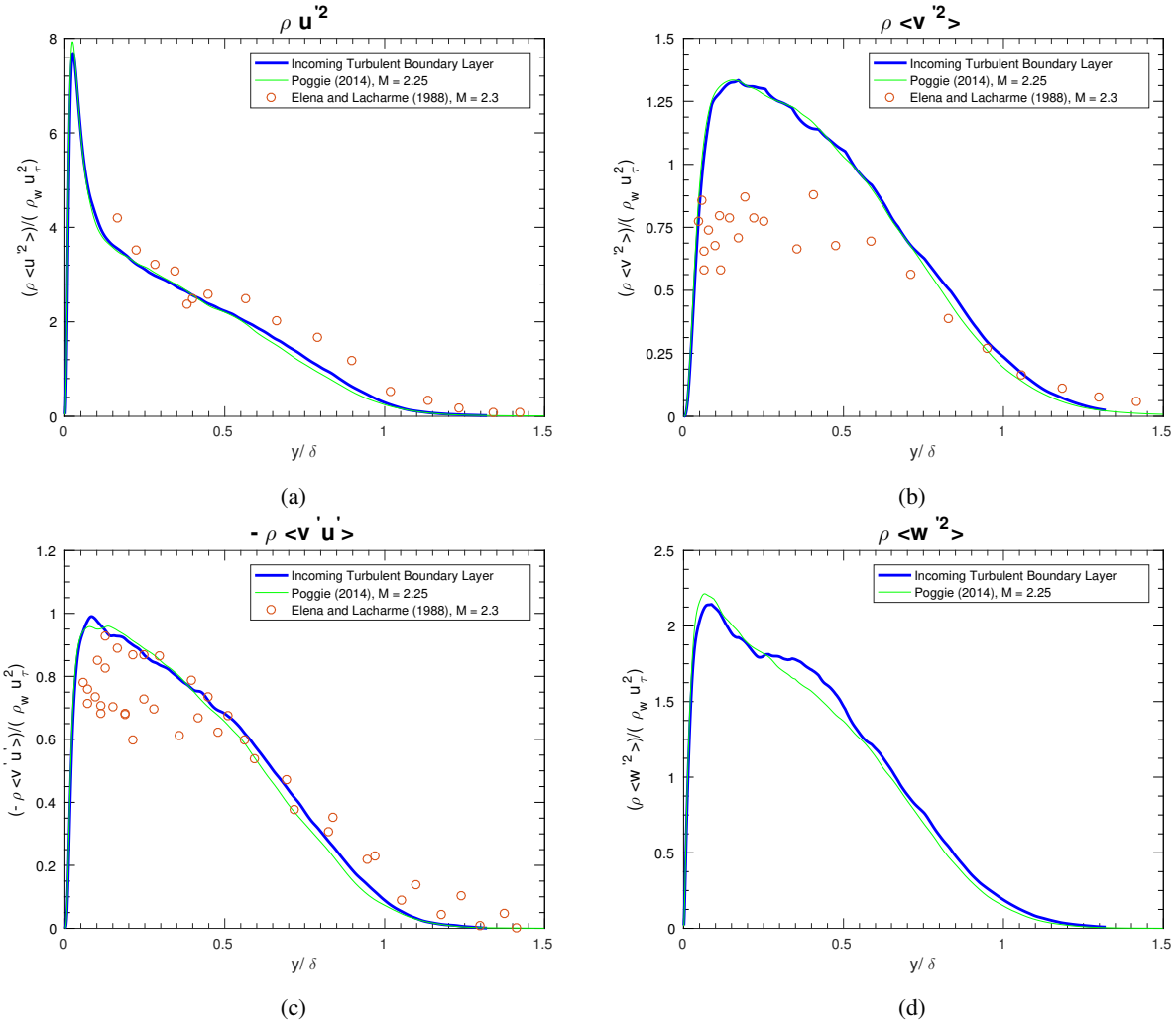

(a)

(b)

(c)

(d)

Figure 4: Reynolds stresses compared to experiments and computations.

III.B. Streamwise Profiles

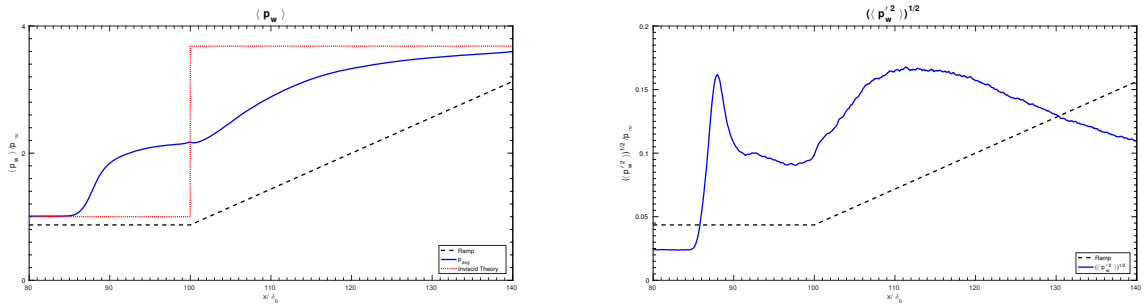

(a) Mean wall pressure. (b) Root-mean-square of the pressure fluctuation.

Figure 5: Streamwise profiles of wall pressure statistics.

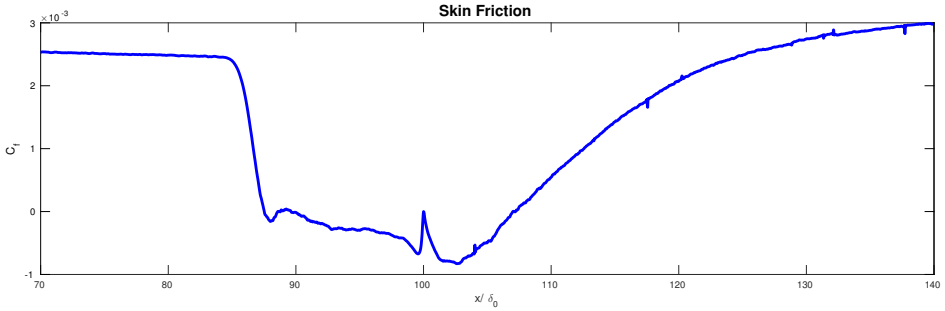

Figure 6: Streamwise profile of mean skin friction coefficient.

Figure 5 shows the mean wall pressure and the root-mean-square of the wall pressure fluctuation. These statistics reflect averages in time, and across the homogeneous z-direction. The pressure contour exhibited the expected profile for a separated shock-wave / boundary-layer interaction. There was an initial rise in pressure from the first shock-wave and then a section of relatively minor pressure increases until the ramp began. Then, the pressure increased towards the inviscidly predicted wall pressure. The plateau in the wall pressure profile was expected for a compression corner with separation; an insufficiently fine grid would miss that feature.[5] There was a peak in the rms of wall pressure under the shock-wave. This gives an indication that there was some unsteadiness associated with the system. The rms profile also showed how the initial shock-wave and the reattachment compression waves differed. The initial shock had a large but concentrated peak in rms whereas the reattachment shock was spread out across a larger area, indicating that reattachment of the separated region was more variable.

The streamwise profile of the mean skin friction is shown in Figure 6. Again, the statistics reflect averages in time and across the span. The skin friction dropped quickly to zero as the incoming turbulent boundary layer separated in the vicinity of the initial shock-wave. The spike at $x = 100$ was due to the discontinuous nature of the compression ramp. As the flow moved up the ramp, the flow reattached, and the skin friction rose above the initial levels.

III.C. Flow Structure

Instantaneous and time-averaged contours for density can be seen in Figure 7. The data for these contours came from the centerplane of the domain ($z/\delta_0 = 5$). The instantaneous contours for density showed the incoming boundary layer interacting with the shock wave, passing through the region of separation and continuing up the ramp. The density contours also showed the structure of the shock-wave and compression waves. The strong initial shock is shown protruding down into the top of the boundary layer where it began to fan out. The compression waves at the rear of the interaction can also be seen making up the second leg of the lambda shock. The time-averaged density contours showed a region of smooth compression, but the instantaneous contour showed that the compression waves were discrete. The contours of the streamwise velocity component more clearly showed how the shock-wave caused separation due to the strong adverse pressure gradient.

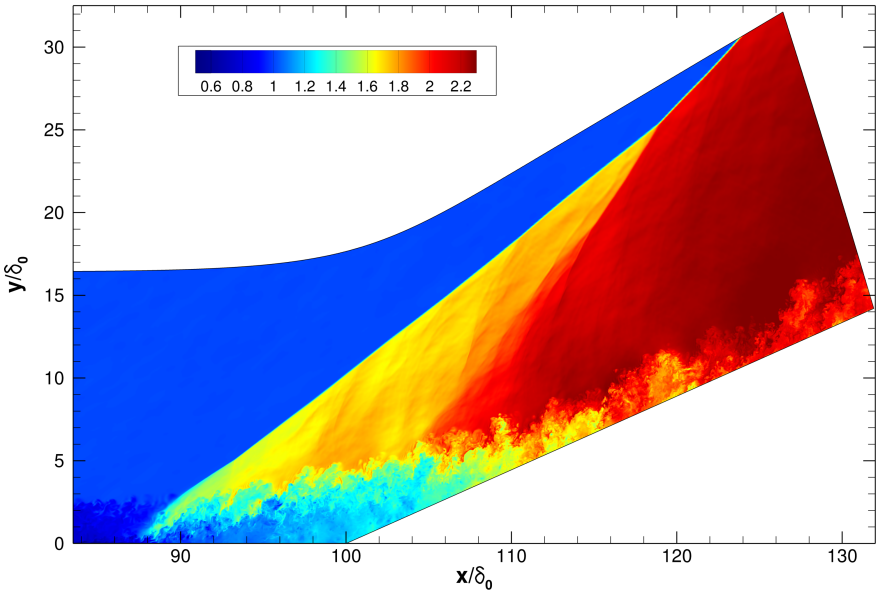

(a) Instantaneous density contour of the centerplane.

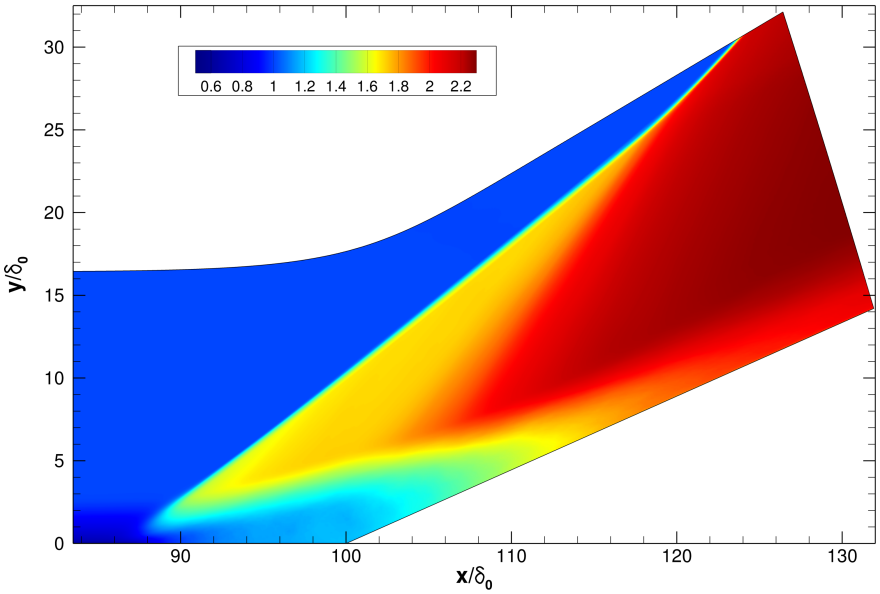

(b) Time averaged density contour of the centerplane.

Figure 7: Density contours in the centerplane ($z/\delta_0 = 5$).

The magnitude of the density gradient is shown in Figure 8. The developed shock wave can be clearly seen extending down to the top of the boundary layer. The figure illustrates how the shock initially developed in front of the compression corner at a shallower angle than would be predicted by inviscid theory due to interactions with the separation bubble. The shock-wave then turned to the angle predicted by the inviscid theory through a collection of compression waves. The time averaged view of this density gradient magnitude shows that the front shock moved slightly, but the compression waves that form the second leg of the traditional lambda shock were quite spread out.

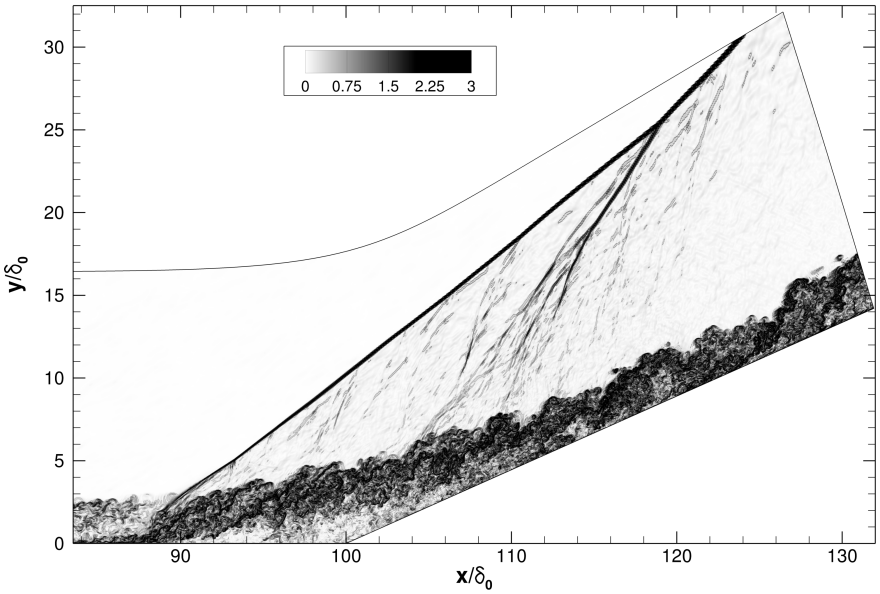

Figure 8: Instantaneous density gradient contour.

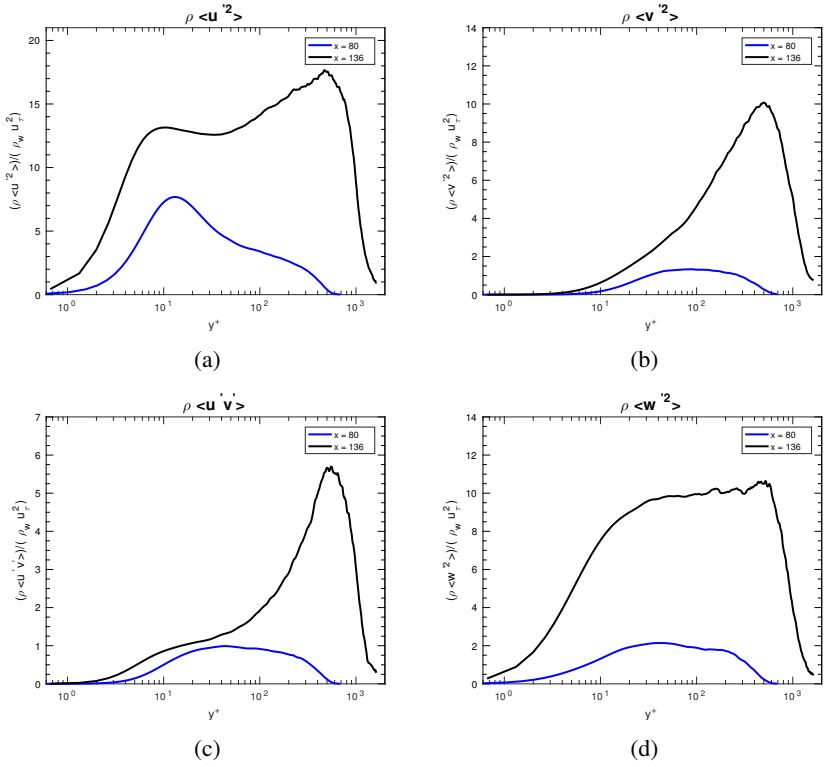

(a) (b) (c) (d)

Figure 9: Reynolds stresses before and after SBLI.

III.D. Turbulence Amplification

Reynolds stresses were examined to look for amplification caused by the SBLI and separation bubble. Such amplification has been observed both in experiments[1] and in computations,[3] and it is an important feature to capture in order to measure the effect of control on the interaction. The turbulent statistics were recorded at two locations along the ramp; one was located before the shock at $x = 80\delta_0$ and the other was at the end of the domain $x = 136\delta_0$. Data were

collected across the span at these stations and averaged over a long period of time. Because the grid was not perfectly perpendicular to the wall at these locations, a volume of data was collected, and the planes were extracted using a simple linear interpolation.

Figure 9 shows all components of Reynolds stresses for the incoming boundary layer and the far after reattachment stations. The amplification in the stresses for all components are qualitatively similar to that of Wu, et al.[3] The amplification factor for the $\rho\langle u'^2\rangle$ component was about 2.3, this is lower than the factor seen by Wu and Martin who saw an increase of about a factor of 3. This is due to the fact that this measurement was taken further downstream from the separated region, 4.7δ for Wu and Martin and 17.6δ for this computation. Additionally, the separated region was larger in this computation, about 9δ, than that of Wu and Martin, about 2δ. The other components saw smaller amplifications as compared to the Wu and Martin's computation as well. The amplification factors for the $\rho\langle v'^2\rangle$, $\rho\langle uv\rangle$, and $\rho\langle w'^2\rangle$ components were 7.6, 5.8, and 5.0 respectively. The domain in the computation was not large enough to allow the Reynolds stresses to fully relax, but it did capture the increases generated by the SBLI.

III.E. Low Frequency Oscillations

Low-frequency oscillations of the shock-wave / boundary-layer system are important because of their contribution to fatigue loading on supersonic aircraft. Altering the characteristics of these oscillations is the future goal for this work so a careful baseline characterization was required. These oscillations were measured and examined for this configuration. When discussing these oscillations, typically the characteristic size is described by the size of the separated region. This can be difficult to define in low Reynolds number flows where the separation and reattachment points are difficult to distinguish.

Data for this computation were collected for 2.8×10^5 time steps at a time interval of $U_\infty \Delta t/\delta_0 = 0.01$. To compute the power spectral density, windows of 50000 points with 50% overlap were used. This gives a resolution of about $f\delta/U_\infty = 0.00454$ where δ is the thickness of the incoming turbulent boundary layer, or $fL_{sep}/U_\infty = 0.04$ where L_{sep} is the size of the separated region. A Strouhal number of 0.04 is greater than the expected peak frequency of the unsteadiness.

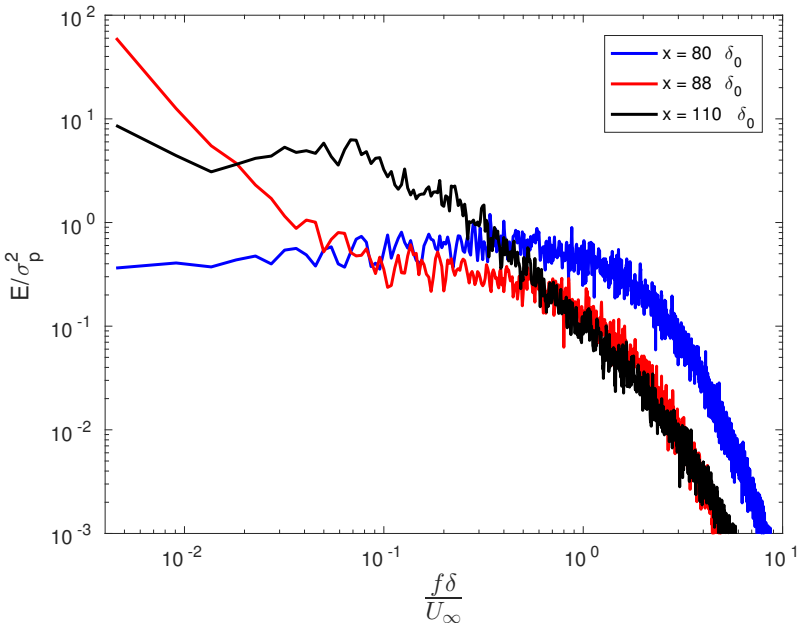

Figure 10: Power spectral density of wall pressure fluctuations for three streamwise locations.

Figure 10 shows the wall pressure spectrum the incoming turbulent boundary layer and the pressure spectrum for the location of maximum wall pressure rms both before and after the compression corner. The spectrum at $x = 80\delta_0$ was upstream of the shock-wave fluctuations and showed little low-frequency content. At $x = 88\delta_0$, the peak in the wall pressure rms before the corner was recorded; there was a large increase in the low frequency content of the signal. At the peak for the wall pressure rms after the ramp at $x = 110\delta_0$ there was a more broadband increase in the low

frequency content. The region with increased amplitude covers more frequencies than the spectrum taken before the corner. It is difficult to precisely determine the frequency of the maximum amplitude of the wall pressure spectrum is located because of the large difference in time scales. However, it is clear that large-scale low-frequency unsteadiness has been generated by the SBLI. Additionally, it appears that the nature of the unsteadiness differs between before and after the ramp.

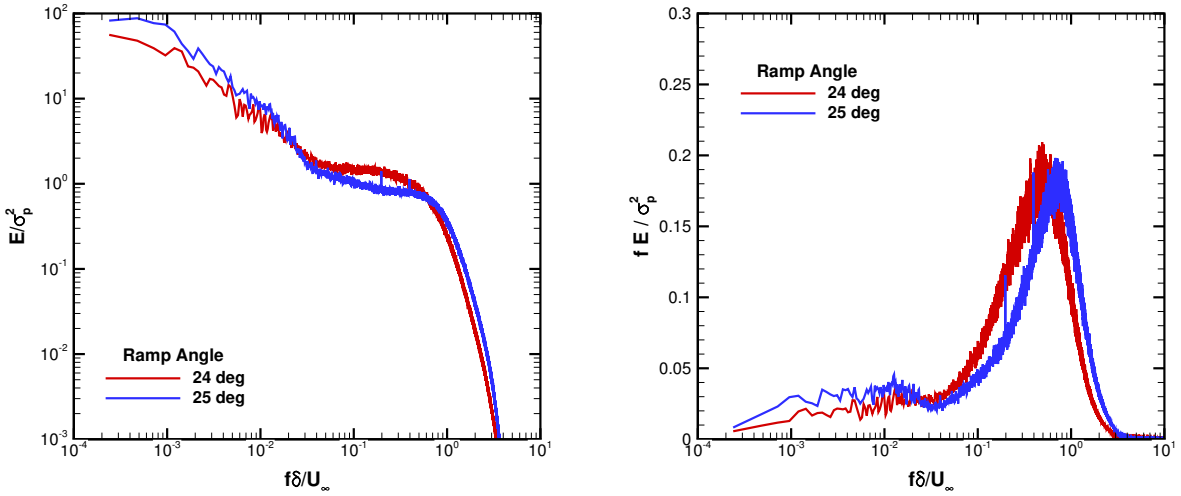

(a) Logarithmic plot

(b) Semilogarithmic plot

Figure 11: Power spectral density of wall pressure fluctuations near the location of maximum fluctuation intensity.

In order to investigate the spectrum of the wall pressure fluctuations for long time scales and low frequencies, additional calculations were carried out on coarser grids for extended runs. In particular, we investigated $24\,\mathrm{deg}$ and $25\,\mathrm{deg}$ ramp configurations on meshes of about 4×10^7 cells. For each case, data were captured for at least 1.1×10^7 iterations, for a total nondimensional time of $U_\infty T/\delta_0 = 1.1 \times 10^5$ ($T^+ = 4.2 \times 10^6$). In terms of a separation scale of about $L_i = 11\delta_0$ for the $24\,\mathrm{deg}$ ramp and the characteristic frequency $f_p = 0.03U_\infty/L_i$, the computation time corresponds to $U_\infty T/L_i = 1.0 \times 10^4$ or $f_p T = 300$. Thus, we have captured approximately 300 cycles of the low-frequency separation shock oscillation.

The spectra were computed by averaging windows of 1×10^6 points, with 50% overlap. The results are shown in Figure 11 for a station close to the maximum pressure fluctuation intensity for each case. The conventional power spectral density is shown on a log-log plot in Figure 11a, and the premultiplied spectrum is shown in Figure 11b. The spectral peak near $f\delta/U_\infty = 0.5$ is believed to correspond to oscillations of the separated shear layer, and the peak near $f\delta/U_\infty = 3 \times 10^{-3}$ ($f_p L_i/U_\infty = 0.03$) to frequency-selective amplification of incoming turbulence by the separation bubble. Note the scaling of the spectra: the slight increase in ramp angle from $24\,\mathrm{deg}$ to $25\,\mathrm{deg}$ leads to an increase in separation bubble scale and a consequent increase in the low-frequency energy content.

It should be noted that this is a very mild separation. Experimental data for strong separation in a blunt fin configuration[21] display low-frequency energy content near $f_p = 0.03U_\infty/L_i$ that greatly exceeds the magnitude of the $f\delta/U_\infty = 0.5$ component. In contrast, experiments on relatively weak compression ramp interactions[22] show a two-peaked spectrum as observed here.

In ongoing work, we are analyzing these long runs in detail. With flow control in mind, we aim to identify precursor flow events that signal large-scale shock motions.

IV. Conclusion

An implicit large eddy simulation was completed for a 24 degree supersonic compression ramp flow. A well-developed turbulent boundary layer encountered a shock-wave generated by the ramp, and a region of separated flow developed. The boundary layer was shown to be fully turbulent through comparison to experiments and other LES computations. The streamwise profiles of pressure and skin friction were also shown. The effect of this separated region on the Reynolds stresses was found to be similar to that observed in other investigations of the effect. The

large-scale, low-frequency fluctuations in pressure were also studied. A spectral peak was observed near a Strouhal number of 0.03, which is in line with the results of other computations and experiments. Using this simulation as a baseline, work can begin on methods of controlling these effects.

Acknowledgments

This project was supported by an award of computer time provided by the DoE INCITE program. This research used resources of the Argonne Leadership Computing Facility, which is a DoE Office of Science User Facility supported under Contract DE-AC02-06CH11357.

The long time-scale runs were supported by grants of High Performance Computing time from the Department of Defense Supercomputing Resource Centers at the Air Force Research Laboratory, the Army Research Laboratory, and the Army Engineer Research and Development Center, provided under a Department of Defense, High-Performance Computation Modernization Program Frontier Project.

References

[1]Smits, A. and Muck, K., "Experimental study of three shock wave/turbulent boundary layer interactions," *Journal of Fluid Mechanics*, Vol. 182, 1987, pp. 291–314.

[2]Bogdonoff, S., "Some Experimental Studies of the Separation of Supersonic Turbulent Boundary Layers," Tech. Rep. 336, Aeronautical Engineering Dept., Princeton Univ., Princeton, NJ, June 1955.

[3]Wu, M. and Martin, M., "Direct Numerical Simulation of Shockwave / Turbulent Boundary Layer Interaction," AIAA Paper 2004-2145, American Institute of Aeronautics and Astronautics, Reston, VA, June 2004.

[4]Adams, N., "Direct numerical simulation of a turbulent boundary layer along a compression ramp at M=3 and $Re_\theta = 1685$," *Journal of Fluid Mechanics*, Vol. 420, 2000, pp. 47–83.

[5]Bisek, N., Rizzetta, D., and Poggie, J., "Plasma Control of a Turbulent Shock Boundary-Layer Interaction," *AIAA Journal*, Vol. 51, No. 8, 2013, pp. 1789–1803.

[6]Settles, G., Fitpatrick, T., and Bogdonoff, S., "Detailed Study of Attached and Separated Compression Corner Flowfields in High Reynolds Number Supersonic Flow," *AIAA Journal*, Vol. 17, 1979, pp. 579–585.

[7]Andreopolous, J. and Muck, K., "Some new aspects of the shock wave boundary layer interaction in compression ramp flows," *Journal of Fluid Mechanics*, Vol. 180, 1987, pp. 405–428.

[8]Verma, S., Manisankar, C., and Akshara, P., "Study of Shock-Wave Boundary-Layer Interaction Control Using an Array of Steady Mirco-Jet Actuators," type of report 9999, Council of Scientific and Industrial Research, National Aerospace Laboratories, address, month 9999.

[9]Verma, S. B., Manisankar, C., and Raju, C., "Control of Shock Unsteadiness in Shock Boundary-Layer interaction on a Compression Corner Using Mechanical Vortex Generators," *Shock Waves*, Vol. 22, 2012, pp. 327–339.

[10]Webb, N., Clifford, C., Porter, A., and Samimy, M., "Control of Oblique Shock Wave-Boundary Layer Interactions Using Plasma Actuators," AIAA Paper 2012–2810, American Institute of Aeronautics and Astronautics, Reston, VA, June 2012.

[11]Gieseking, D., J., E., and Choi, J., "Simulation of a Mach 3 24-Degree Compression-Ramp Interaction using LES/RANS Models," AIAA Paper 2004-5541, American Institute of Aeronautics and Astronautics, Reston, VA, July 2003.

[12]Dolling, D., "Fluctuation Loads in Shock Wave/Turbulent Boundary Layer Interaction: Tutorial and Update," AIAA Paper 1993-0284, American Institute of Aeronautics and Astronautics, Reston, VA, January 1993.

[13]Poggie, J., Bisek, N., Leger, T., and R., T., "Implicit Large-Eddy Simulation of a Supersonic Turbulent Boundary Layer: Code Comparison," AIAA Paper 2014-0423, American Institute of Aeronautics and Astronautics, Reston, VA, January 2014.

[14]Poggie, J., Bisek, N., and R., G., "Resolution effects in compressible, turbulent boundary layer simulations," *Computers and Fluids*, Vol. 120, 2015, pp. 57–69.

[15]Georgiadis, N., Rizzetta, D., and Fureby, C., "Large-Eddy Simulations: Current Capabilities, Recommended Practices, and Future Research," *AIAA Journal*, Vol. 48, No. 8, 2010, pp. 1773–1784.

[16]Rizzetta, D. P. and Visbal, M. R., "Large-Eddy Simulation of Supersonic Boundary-Layer Flow by a High-Order Method," *International Journal of Computational Fluid Dynamics*, Vol. 18, No. 1, 2004, pp. 15–27.

[17]Pirozzoli, S., Grasso, F., and Gatski, T. B., "Direct Numerical Simulation and Analysis of a Spatially Evolving Supersonic Turbulent Boundary Layer M = 2.25," *Physics of Fluids*, Vol. 16, No. 3, 2004, pp. 530–545.

[18]Mullenix, N. J., Gaitonde, D. V., and Visbal, M. R., "Spatially Developing Supersonic Turbulent Boundary Layer with a Body-Force-Based Method," *AIAA Journal*, Vol. 51, No. 8, 2013, pp. 1805–1819.

[19]Poggie, J., "Large-Scale Structures in Implicit Large-Eddy Simulation of Compressible Turbulent Flow," AIAA Paper 2014-3328, American Institute of Aeronautics and Astronautics, Reston, VA, June 2014.

[20]Éléna, M. and Lacharme, J. P., "Experimental Study of a Supersonic Turbulent Boundary Layer Using a Laser Doppler Anemometer," *Journal Mécanique Théorique et Appliquée*, Vol. 7, 1988, pp. 175–190.

[21]Poggie, J., Bisek, N. J., Kimmel, R. L., and Stanfield, S. A., "Spectral Characteristics of Separation Shock Unsteadiness," *AIAA Journal*, Vol. 53, No. 1, 2015, pp. 200–214.

[22]Thomas, F. O., Putnam, C. M., and Chu, H. C., "On the Mechanism of Unsteady Oscillation in Shock Wave/Turbulent Boundary Layer Interaction," *Experiments in Fluids*, Vol. 18, 1994, pp. 69–81.